Impact of ZIF flexibility for aromatic vapor capture

T. Aumond, C. Daniel, C. Collomb, K. Dedecker, M. Drobek, A. Julbe, D. Farrusseng

Impact of ZIF flexibility for aromatic vapor capture

Thibaud Aumond,[a,*] Cécile Daniel,[a] Corentin Collomb,[a] Kevin Dedecker,[b] Martin Drobek,[b] Anne Julbe,[b] David Farrusseng[a]

[a] Université de Lyon, Université Claude Bernard Lyon 1, CNRS, IRCELYON - UMR 5256, Villeurbanne 69626, France

[b] Institut Européen des Membranes (IEM), CNRS, ENSCM, Univ Montpellier, Place Eugène Bataillon, 34095 Montpellier, France

* Corresponding author: thibaud.aumond@ircelyon.univ-lyon1.fr

KEYWORDS: zeolitic imidazolate frameworks, BTEX, adsorption/desorption mechanism, π-π stacking

TOC

ZIF-8, a flexible MOF triggered by guest-host interactions, has been tested for BTX adsorption/desorption using static and dynamic methods. It exhibits excellent retention capacity at moderate temperatures due to the local mobility of the linkers.

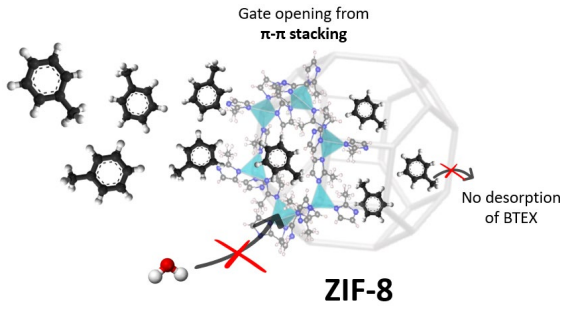

ABSTRACT

Technological innovations allowing the capture of volatile organic compounds (VOCs), in particular aromatic compounds (BTEX), continue to be sought. Activated carbon (AC) is a widely-used adsorbent, but upon moderate temperature increases, typically 50 °C, it tends to release accumulated VOCs and thereby contribute to air pollution peaks. We evaluate herein the adsorption performances of ZIF-7 synthesized from a new and greener protocol as well as ZIF-8. These two MOFs exhibit flexibility triggered by guest-host interactions, for the adsorption of benzene, toluene and *p*-xylene (BTX). The desorption capacity of different materials at various temperatures is examined. Adsorption/desorption performances are evaluated using both the static method (volumetric analysis) and the dynamic method. The latter allows for the co-adsorption of the pollutant in the presence of water. Unlike traditional AC, ZIFs demonstrate unaffected adsorption performance in the presence of water. Both AC and ZIF-7 undergo significant desorption at low temperatures (55 and 93 % of adsorbed toluene, respectively), potentially releasing high concentrations of VOCs when exposed to solar radiation, which eliminates the possibility of its application for indoor air treatment. Remarkably, ZIF-8 does not show significant BTX desorption for temperatures below 50°C (14%), while maintaining excellent regeneration characteristics at higher temperatures. We propose that this specific property can be depicted by a local dynamic-motion mechanism. Toluene is strongly diffusion-controlled, requiring the overcoming of a high energy barrier to cross the narrow six-membered ring aperture, while the size of the aperture is reduced by a ratio of the linker induced by the toluene packing in the sodalite (SOD) cavity.

I. INTRODUCTION

Benzene, toluene, ethylbenzene and xylenes, collectively known as BTEX, are airborne volatile organic compounds (VOCs) recognized as toxic pollutants responsible for both indoor and outdoor air pollution, leading to various health issues.[1,2,3,4] Specifically, benzene is well documented for its carcinogenic effects.[5] The primary source of BTEX in urban environments is vehicle exhaust, with concentration peaks also observed during forest fires.[6,7]

Adsorption of VOCs, particularly BTEX, onto microporous solids such as activated carbons (AC)[8,9,10] and hydrophobic zeolites[11,12,13] is commonly employed in dynamic systems, including fixed-bed (chromatographic) columns and coatings on rotor concentrators.[14] Kim *et al.* established criteria and metrics derived from the benzene adsorption isotherm, including the partitioning coefficient (K_H) and equilibrium adsorption capacity at low pressure, to facilitate the preliminary screening of potential adsorbent candidates under relevant VOC concentration conditions. A ranking of 73 adsorbent candidates from literature data indicates that activated carbons are suitable for benzene removal in adsorption/desorption cycling processes.[15] Another class of porous materials, metal-organic frameworks (MOFs), has been widely studied for VOC adsorption. Due to its high specific surface area, MIL-101 was studied in 2011 for BTEX adsorption by Zhao et al., leading to an adsorption capacity of *p*-xylene of 10.9 mmol g^{-1} at 15 °C and 6 mbar.[16] Other MOFs have been tested for BTEX adsorption such as UiO-66, HKUST-1, and MOF-5 for example.[17,18,19] Nevertheless, the choice of highly hydrophobic MOFs appears as a determinant criterion for VOC capture since water concentration is not neglectable in the atmosphere, and moisture reduces the available sites for VOC adsorption.[20] Furthermore, the stability of the MOF can be lowered in the presence of water.[21,22] Recently, He *et al.* highlighted the exceptional performance of MOFs, specifically BUT-53/58, in terms of adsorption capacity at a benzene concentration of 10 ppm with notable breakthrough times

even in the presence of high humidity levels.[5] Another category of MOFs, Zeolite-Imidazolate Frameworks (ZIFs) and more precisely ZIF-7 and ZIF-8 are well known as highly hydrophobic materials.[23]

In contrast to industrial HVAC (heating, ventilation and air-conditioning) systems that utilize swing adsorption-desorption processes,[24,25] passive VOC systems, such as removable activated carbon filters used in individual air-treatment devices or vehicles, are not regenerated and must be regularly replaced with fresh filters. While adsorption capacity is a critical criterion determining the filter's usage time, the desorption of VOCs from the filter back into the environment presents a significant challenge. A slight increase in temperature (i. e. up to 50 °C) can lead to the rapid desorption of VOCs that have accumulated over time, resulting in elevated VOC concentrations in the surrounding air.[26] This issue is particularly pronounced in automotive air-treatment systems, for which sudden temperature increases (e.g., due to parking a car in direct sunlight) can exacerbate the problem. In prototype tests for vehicle applications, Alvarez *et al.* measured nearly instantaneous VOC release from activated carbons and MOFs when the temperature was raised from room temperature to 50°C. The results highlight the need for improved materials and designs that mitigate the risks associated with VOC desorption in passive air-treatment systems.[27]

We anticipated that MOFs with flexibility triggered by guest-host interactions could exhibit enhanced adsorption strength and, consequently, reduce or slow down the release of VOCs subjected to a temperature increase.[28,29] ZIF-7 and ZIF-8, which possess the same sodalite (SOD) topology, are obtained under mild synthesis conditions making them sustainable for the environment.[30] As they exhibit two different types of structural flexibility upon guest adsorption,[31] they were chosen as the study materials. ZIF-8, composed of Zn^{2+} cations and 2-methylimidazole ligands, is renowned for its gate-opening mechanism, also referred to as local dynamic motion or the trap-door effect. This phenomenon involves the

rotation of the imidazolate linkers, which expands the pore aperture of the six-membered ring windows from 3.4 to 4.1 Å. This rotation is observable under high pressure or during gas adsorption uptake. [32,33] In contrast, ZIF-7 "breathing" is associated with a phase-to-phase transition involving a crystallographic change from a high-density phase II structure with triclinic symmetry (narrow pore, np) to a low-density phase I structure with trigonal symmetry (large pore, lp).[34,35] This phase transition upon adsorption is accompanied by a significant adsorption/desorption hysteresis, evidencing stronger entrapment of guest molecules. [36,37] For VOC preconcentration samplers, Lv *et al.* found that benzene is more difficult to desorb in ZIF-7 than in Tenax (a state-of-the-art adsorbent), attributing this phenomenon to the framework flexibility.[38]

In this study, we develop a new synthetic route for ZIF-7 that does not necessitate a heating step, improving its synthesis from an environmental point of view. We then demonstrate through static and dynamic adsorption/desorption experiments that BTEX molecules are difficult to desorb from ZIF-8 upon heating below 100°C. Conversely, ZIF-7 and the reference high surface-area AC allow for significant desorption of BTEX in the above temperature range. Moreover, we show that the relative humidity level does not significantly influence BTEX adsorption/desorption when using ZIF-8.

II. EXPERIMENTAL

II.1) Materials

Activated carbon (AC) (SP-Defense, Honeywell) and ZIF-8 (MOFapps) were purchased and post-processed as described to allow proper chromatographic studies. The materials were compacted using a press at 2 tons for 2 minutes, yielding a tablet of 30 mm diameter and 3 mm thickness, and then this tablet was crushed and sieved to obtain homogeneous particles with diameters between 300 µm and 600 µm.

ZIF-7 was synthesized according to this newly developed synthesis protocol. In a 250-mL round-bottomed flask, 1.2 g (10 mmol) of benzimidazole and 1.36 g (7 mmol) of $Zn(NO_3)_2 \cdot 6H_2O$ were dissolved in 100 mL of acetone. After complete dissolution, 10 mL of ethylenediamine was added to the mixture during placement in an ice bath to prevent acetone evaporation. The solution was then left at room temperature for 2 hours under continuous stirring. Subsequently, the mixture was centrifuged at 9000 rpm for 20 minutes to separate the solid material from the liquid. The resulting ZIF-7 was dispersed in 30 mL of DMF to eliminate any remaining reactants. This washing procedure was repeated three times using DMF and twice with MeOH. The residue was then left at room temperature overnight. ZIF-7 was sieved to obtain homogeneous particles with diameters between 300 µm and 600 µm, similar to the two other materials. After heating to 150°C under vacuum to remove all contaminants, ZIF-7 in phase II configuration was obtained.

II.2) Characterization of the adsorbents

X-ray diffraction (XRD) patterns were recorded using a Bruker (Siemens) D5000 diffractometer. Diffractograms were collected in the 2θ range of 5° to 50° with a step size of 0.02° and a counting time of 1 second per step, using CuKα radiation (λ = 1.54059 Å).

Elemental analysis was performed to quantify the atomic amounts of carbon, hydrogen and oxygen in carbonaceous materials using a Flash 2000 Thermo instrument. Prior to analysis, the samples were dried at 100°C to remove adsorbed water molecules. Nitrogen physisorption measurements were conducted using a Microtrac Belsorp Mini X instrument at 77 K. Before the physisorption measurements were carried out, approximately 50 mg of the sample was outgassed overnight under vacuum at a specific temperature based on the thermal stability of the sample: 140°C (ZIFs) or 300°C (AC). Experiments were performed for relative pressures (P/P_0) between 0 and 1. Each data point was recorded with a pressure variation lower than 0.3% for 300 seconds as the equilibrium criterion. The pore size distribution of AC was calculated from the CO_2 isotherm measured at 298 K using the Grand Canonical Monte Carlo (GCMC) model for non-graphitic carbon materials.

II.3) Static adsorption/desorption methods

To evaluate the sorption capacities of the different porous materials, volumetric static adsorption/desorption experiments of the BTX compounds were initially performed using a Microtrac Belsorp Max II apparatus. Isotherms were obtained by applying a defined tabulated pressure. Thermodynamic equilibrium was considered achieved when the total pressure variation within the cell was lower than 0.3% for 300 seconds. Isotherms were performed at three different temperatures (20, 40 and 60 °C) and analyzed by Polanyi's adsorption potential theory to assess whether thermodynamic equilibrium had been reached or not.[39] This theory yields a characteristic function that is representative of the fluid/solid system under investigation. In practice, the adsorbed phase volume (taking into account the molar volume of the studied molecule at the experimental temperature) is plotted as a function of the chemical potential μ (Equation 1):

$$\text{Equation 1} \qquad \mu = RTln\left(\frac{P}{P_0}\right)$$

Here, R is the gas constant (8.314 J K^{-1} mol^{-1}), T the experiment temperature (K), P the equilibrium pressure (Pa), and P_0 the saturation pressure at the given temperature. P/P_0 can be directly read from the isotherms.

Due to instrumental limitations, isotherms performed at 60°C were terminated at $P/P_0 = 0.4$. Prior to the adsorption/desorption experiments, each sample was degassed overnight, similarly to the N_2 adsorption (77 K) measurements. This degassing procedure was implemented to remove any contaminants from the materials.

II.4) Dynamic adsorption/desorption experiments

Dynamic (breakthrough) adsorption experiments were conducted using a custom-built setup described elsewhere.[40] A scheme of the setup is available in the supporting information (Figure S1). For dynamic adsorption experiments, toluene has been used as a model compound, as toluene, benzene, and *p*-xylene are all aromatic compounds and have similar kinetic diameters.[41] Prior to the adsorption process, materials were activated under N_2 flow at 140°C to remove any previously adsorbed molecules using the oven. The concentration of the contaminant in the inlet flow (C_0) was measured by a bypass of the column. The column was made by filling a glass tube of 4 mm internal diameter with an 8-cm height of nanoporous material, corresponding to around 500 mg of adsorbate, depending on the density of the powder. Breakthrough experiments were performed at atmospheric pressure and a constant temperature of 20°C controlled by a heated bath. Two conditions were studied: dry and wet. For dry conditions, a 200 mL min^{-1} flow of N_2 (contact time $\tau = 0.3$ sec) containing 1000 ppm of the adsorbate (corresponding to 8.89×10^{-6} mol min^{-1} of BTX) was achieved by a GasMix™ (Alytech) gas diluter apparatus, designed as VOC FEED, LIQMIX in the scheme S1. The adsorbate concentration of the outlet flow (C) was evaluated using an FTIR detector. For the quantitative measurements of toluene, the classical least squares technique was used with an

FTIR Nicolet iS20 spectrometer. Before every measurement, a background scan was performed. For toluene quantitative analyses, and to avoid taking into account the water bands in the spectra, the region used was between 2688.16 and 3211.62 cm^{-1} (Figure S2). The toluene calibration curve was obtained using toluene concentrations between 20 and 1045 ppm, 12 spectra were used for the calibration and 11 spectra for validation (Figure S3). In order to obtain toluene concentrations in mol min^{-1}, the following equation was used (Equation 2):

$$\text{Equation 2} \qquad [C] = \frac{[ppm] \times \frac{Total\ flow}{V_M \times C_0}}{[ppm]_0}$$

Experiments under wet conditions were conducted under a high relative humidity (RH) corresponding to a humid climate (i.e. = 70%). For these experiments, a flow containing water vapor, obtained by bubbling N_2 gas in water, was mixed with the flow from the GasMix™ diluter containing the adsorbate. The final concentration was set to 1000 ppm. Considering the water vapor pressure at 20°C (2.33 kPa), the resulting final water vapor pressure at 70% RH was 1.63 kPa.

After the adsorption step was completed, desorption measurements were carried out to determine how strongly the adsorbates were trapped within the porous solids. The column was heated gradually under N_2 (200 mL min^{-1}) at temperatures gradually raised from 50°C to 150°C, with three plateaus at 50, 100 and 150°C.

In order to compare the different quantities of molecules adsorbed, every breakthrough graph is presented for 1 gram of dried adsorbent.

III. RESULTS

III.1) Static adsorption/desorption of BTX and water

The textural and structural characterizations of ZIF-7 and ZIF-8 are presented and discussed in supporting information (S4).

As anticipated for the highly hydrophobic ZIF-7 and ZIF-8, no water adsorption is observed across the entire range of RH ($0<P/P_0<1$) (Figure S5a). In contrast, activated carbon (AC) exhibits distinct adsorption behavior. Whereas no water adsorption is detected for RH below 50%, AC adsorbs water at a threshold of 55%. At 70% RH, AC adsorbs 21 mmol g^{-1} of water, with its total water adsorption capacity reaching 31 mmol g^{-1}. The desorption branch for AC does not match the adsorption branch, resulting in a hysteresis loop with a triangular-like shape. A desorption observed at 0.5 P/P_0 is attributed to the evaporation of unstable water condensate from the mesoporous pores.[42]

Static adsorption isotherms of benzene, toluene and *p*-xylene were performed at three different temperatures on ZIF-7 and ZIF-8. For comparison, toluene isotherms on AC are presented in Figure S5b, showing a decrease in the total adsorbed amount of toluene. Between 4.5 and 5 mmol g^{-1} of toluene are adsorbed depending on the temperature.

Isotherms of BTX adsorption on ZIF-7 are presented in Figures 1a-c. The shape of the isotherm is independent of the adsorbate, and the desorption branch differs from the adsorption branch. This can indicate high material flexibility. The hysteresis is related to the stabilization of the structure with the adsorption of BTX, and more energy is needed to desorb the adsorbate. The thermodynamic equilibrium was verified by performing BTX adsorption isotherms at three different temperatures and applying Polanyi's adsorption potential theory. As shown in Figures

1d-f, thermodynamic equilibrium is nearly achieved for all BTX compounds adsorbed on ZIF-7, as evidenced by the superposition of the three resulting Polanyi curves.

For all three adsorbate molecules on ZIF-7, a phase transition from the narrow pores (phase II) to the large pores (phase I) is observed from the isotherms. Nevertheless, and depending on the aromatic adsorbate, the phase transition is obtained at different temperatures. At relatively low concentrations, approximately five to six molecules per SOD cage can be adsorbed when ZIF-7 features phase II pores. For the less bulky benzene, an increase in adsorbate concentration triggers the transition to phase I pores, allowing the adsorption of around 17 benzene molecules per cage at both 20 and 40°C (Figure 1a). In the case of toluene, around 17 molecules per SOD cage are absorbed at 40°C. In contrast, at 20°C, fewer molecules are adsorbed, likely because the phase II to phase I transition is easier at higher temperatures. The bulkier *p*-xylene molecule induces a phase II to phase I transition only at the highest temperature (40°C), leading to the adsorption of around 15 molecules. Polanyi's adsorption potential curves seem to indicate that equilibrium is not fully achieved at 20°C for the highest relative pressures ($P/P_0 > 0.7$). Compared to other adsorbates studied, fewer *p*-xylene molecules are adsorbed (three to four molecules per SOD cage for phase II, and 15 molecules for phase I). We can propose that the presence of methyl substituents on the aromatic ring limits the π-π stacking between the guest molecules and the aromatic ring of ZIF-7, the limiting effect of two substituents (*p*-xylene) being more pronounced than for one substituent (toluene). Hence, we can suggest that the ability of guest molecules to pack into the narrow pore phase contributes to the phase transition to the large-pore phase. When fewer guest molecules are packed in, which is typically the case for *p*-xylene, additional thermal energy is required to open the structure.

It is possible to determine the expected adsorption capacity at a given temperature from isotherm data. Table 1 presents the adsorption capacities of the different materials at a concentration of 1000 ppm (0.1 kPa).

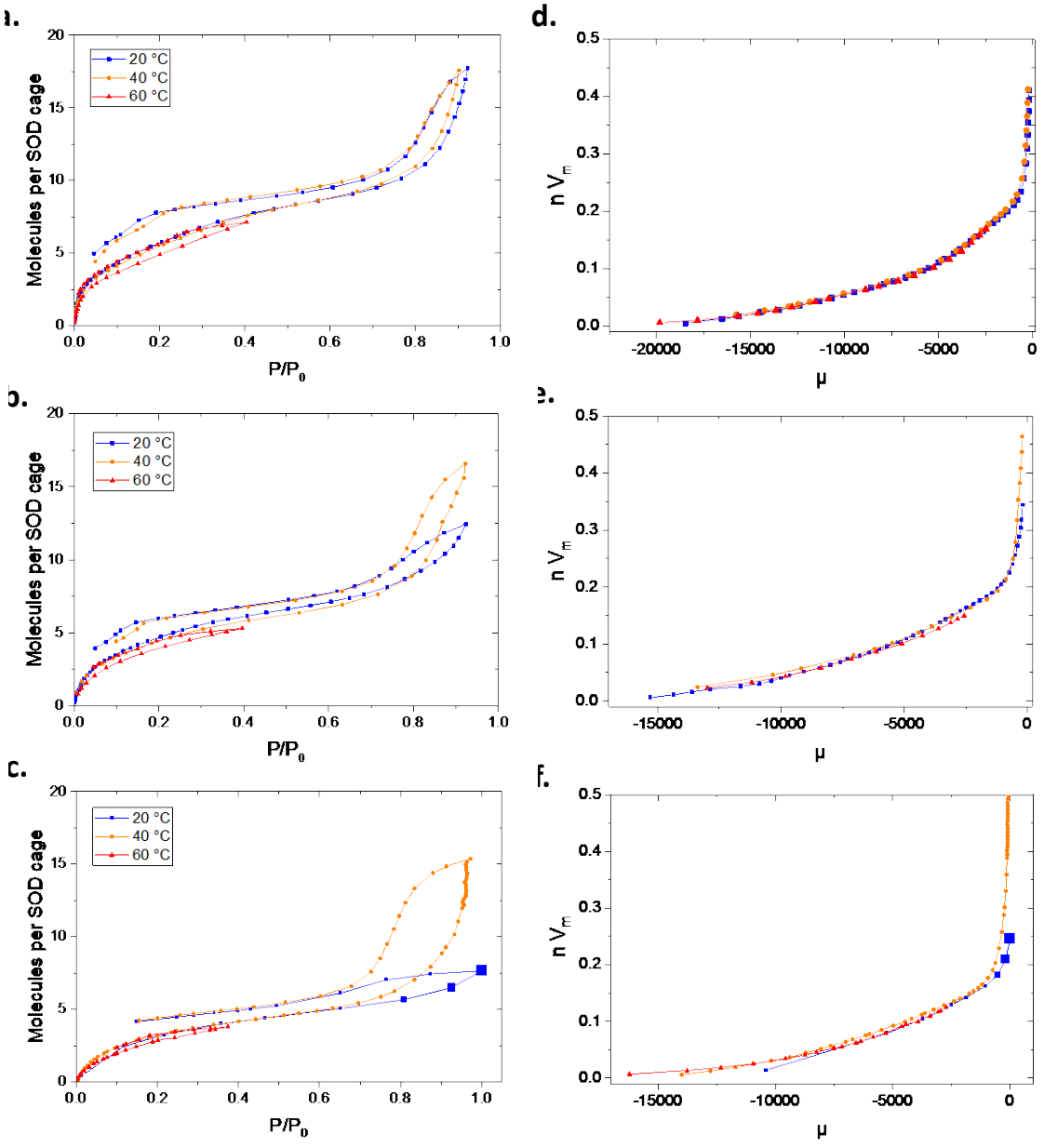

Figure 1. Benzene (a), toluene (b) and *p*-xylene (c) physisorption isotherms over ZIF-7 at different temperatures, accompanied by the corresponding Polanyi adsorption potential

theory plots (d, e, f). To guide the reader, the three last dots of the isotherm and of the resulting Polanyi plot obtained from *p*-xylene at 20°C have been enlarged.

Table 1. Adsorption capacities of different adsorbents for BTX at different temperatures at 0.1 kPa (1000 ppm).

Method	Adsorbate	T (°C)	Adsorption capacity (mmol g^{-1})		
			TA80	ZIF-7	ZIF-8
Static	Benzene	20	/	0.50	0.11
		40	/	0.30	0.03
		60	/	0.12	<0.04
	Toluene	20	4.4	0.55	0.65
		40	4.0	0.30	0.75
		60	3.2	<0.2	0.17
	p-Xylene	20	/	0.25	0.75
		40	/	0.37	1.3
		60	/	0.17	1.1
Dynamic	Toluene	20	4.3	0.8	1.5

Surprisingly, and in contrast to ZIF-7, an increase in temperature results in higher adsorption capacities for ZIF-8 for toluene and xylene, in contradiction with thermodynamic principles (Figure 2b-c). Application of Polanyi's adsorption potential theory confirms that thermodynamic equilibrium is not achieved at low pressure despite the strict equilibrium criteria established in the measurement protocol (Figure 2e-f). For adsorption potentials of about -5.000, adsorption branches for 40 and 60°C match for toluene and *p*-xylene, indicating that equilibrium has been achieved for these measurements. This condition corresponds to relative pressure windows of 0.2-0.95 and 0.15-0.95 for toluene and *p*-xylene, respectively, for which saturation is achieved. At 60°C, when the isotherm most closely approaches saturation ($P/P_0 = 0.4$), six molecules of toluene and *p*-xylene per SOD cage are adsorbed, followed by a plateau. Similar conclusions can be drawn for benzene (Figure 2a), for which around seven molecules are adsorbed. The lower number of adsorbates in the SOD cage of ZIF-8 with toluene

and *p*-xylene can be attributed to the larger size of substituted aromatics and their lesser ability to pack into the SOD cavity.

In contrast to the ZIF-7 isotherms, for which the desorption branches monotonously decrease with the relative pressure, irrespective of adsorbates, the desorption branches for ZIF-8 are rather flat. This is particularly the case for isotherms at 20°C, for which desorption can hardly be detected until $P/P_0 = 0.05$, which corresponds to the measurement limits of the instrument. The fact that benzene, toluene and *p*-xylene can hardly desorb at low vapor pressure (between 2 and 9% desorbed for $P/P_0 = 0.1$) indicates a strong stabilization of the adsorbates in ZIF-8 SOD cavities.

Co-adsorption of adsorbates is not possible using static conditions in standard equipments. Dynamic adsorption experiments allow co-feeding to study the impact of relative humidity on BTX adsorption. Furthermore, the desorption of the pollutant can be followed at different temperatures and atmospheric pressure.

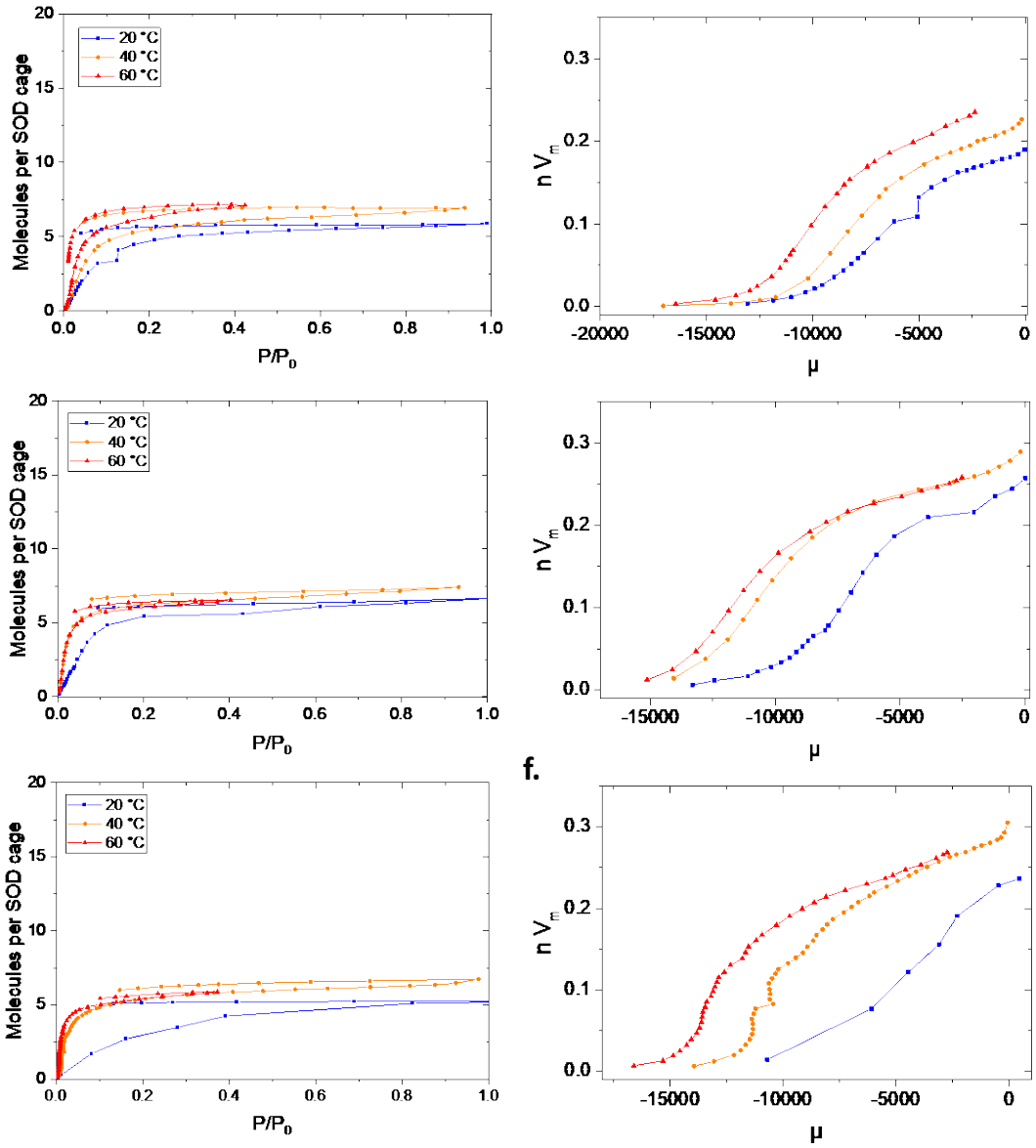

Figure 2. Benzene (a), toluene (b) and *p*-xylene (c) physisorption isotherms over ZIF-8 at different temperatures, accompanied by the resulting Polanyi adsorption potential theory plots (d, e, f).

III.2) Dynamic adsorption/desorption of toluene with 70% relative humidity

To mimic relevant adsorption processes, breakthrough experiments were conducted at 20°C under wet streams (RH = 70%, approximating ambient RH) containing 1000 ppm of toluene. This concentration can be related to the value obtained from static isotherms at 0.1 kPa. Very distinct adsorption profiles were observed depending on the adsorbent (Figure 3). As shown in Figure 3a, toluene adsorption on activated carbon (AC) occurs in three distinct phases: *i*) during the first 8 h g^{-1} both water and toluene are adsorbed, which is consistent with the static isotherms described previously. Indeed, at a relative humidity of 70%, AC adsorbs around 21 mmol g^{-1} of water according to the isotherm. Then, *ii*) after 9 h g^{-1}, water molecules begin to desorb (roll-up) while toluene continues to be adsorbed. In contrast to the experiment without RH, where the breakthrough profile exhibits a perfect S-shape (Figure S6), diffusional constraints emerge toward the end of toluene adsorption ($t \approx 15$ h g^{-1}), likely due to the presence of water molecules impeding the adsorption process. Finally, *iii*) after 28 h g^{-1}, adsorption ceases for both water and toluene. Integration of the curves makes it possible to calculate that 4.3 mmol g^{-1} of toluene is adsorbed (Table 1), while the quantity of remaining water molecules is 1.3 mmol g^{-1}.

The adsorption profiles of ZIF-7 and ZIF-8 are rather similar but differ significantly from that of AC. As expected, no water adsorption occurs on either ZIF material, resulting in an immediate water breakthrough for both of the ZIFs (Figures 3b, c). Regarding toluene adsorption, the curved profile of the C/C(0) (t) plots clearly indicates major diffusional constraints for both ZIF-7 and ZIF-8. Nevertheless, a notable difference between the two ZIFs was evidenced for the equilibrium time. For ZIF-7, the adsorption process lasts approximately 16 h g^{-1}, while for ZIF-8, the adsorption time is more than three times longer. At a concentration

of 1000 ppm, at least 50 h g^{-1} is required to reach thermodynamic equilibrium. This extended equilibration time for ZIF-8 in dynamic conditions is in line with the observation that equilibrium was rarely achieved during the adsorption isotherm measurements. The final adsorption capacities of ZIF-7 and ZIF-8 for toluene respectively equal 0.8 mmol g^{-1} and 1.5 mmol g^{-1} (Table 1), which highlights that the adsorption capacity of ZIF-8 is nearly double that of ZIF-7.

As far as ZIF-7 is concerned, for a concentration of 1000 ppm (0.1 kPa), the phase transition from narrow phase II pores to large phase I pores does not occur, and 3.0 molecules of toluene per SOD cage are adsorbed. This value only slightly differs from the result obtained from the static experiment, with 2.2 molecules of toluene adsorbed per SOD cage. On the contrary, the values obtained for ZIF-8 highly differ: 4.1 molecules per SOD cage are adsorbed during the breakthrough experiment, which is more than twice as high as the 1.8 molecules adsorbed during the static experiment. ZIF-8 allows the adsorption of 37% more toluene molecules per SOD cage in comparison with ZIF-7.

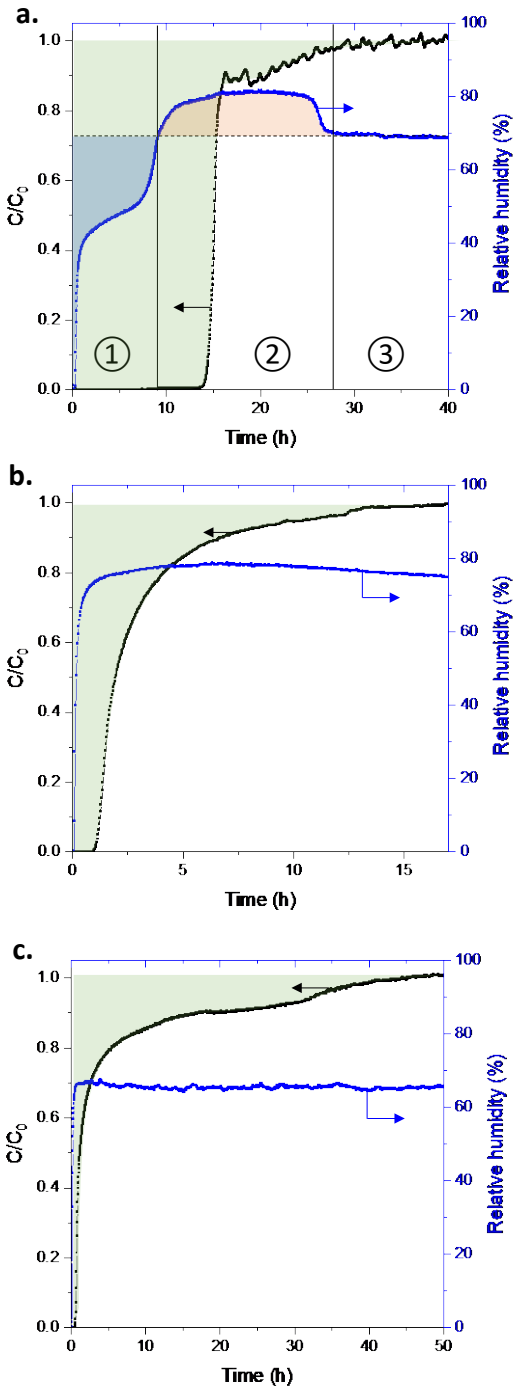

Figure 3. Breakthrough profiles of toluene (1000 ppm) at 20°C on AC (a), ZIF-7 (b) and ZIF-8 (c) in the presence of water (RH = 70%) with a total flow rate of 200 mL min^{-1}. Green represents the toluene adsorption, blue the water adsorption, and orange the water desorption. Bed of the adsorbent = 8 cm height. *Time is reported for 1 gram of adsorbent.

Desorption profiles were recorded by heating the column at different temperatures under inert flow after the adsorption experiments to simulate the regeneration of the adsorbents (Figure 4). The results reveal distinct desorption behaviors for each material. AC undergoes relatively little desorption at ambient temperature. Nevertheless, an increase in temperature to 40 and 50°C leads to higher toluene desorption, with 2.4 mmol g^{-1} of toluene desorbed at temperatures ≤ 50°C, representing 55% of the initial adsorption. Complete regeneration of AC requires a temperature of 150°C. At 100°C, 1.03 mmol g^{-1} (or 25%) of the toluene remains within the porous system. In contrast, ZIF-7 exhibits predominantly weak interactions, as evidenced by the desorption of 93% (0.7 mmol g^{-1}) of the adsorbed toluene at 40°C, with complete regeneration achieved at 100°C. ZIF-8 results are very different. In contrast to ZIF-7 and AC, which desorb toluene at low temperatures, only 14% of the toluene (0.2 mmol g^{-1}) is desorbed at temperatures up to 50°C for ZIF-8, while an increase of temperature to 100°C allows for the desorption of over 70% of the remaining toluene. Complete regeneration of ZIF-8 requires a temperature of 150°C to remove the remaining aromatic molecules.

After this first adsorption/desorption cycle, another partial adsorption experiment was performed, and no changes in the breakthrough curve were detected, confirming that the adsorbent can be reused without modification of its adsorption capacity (Figure S7).

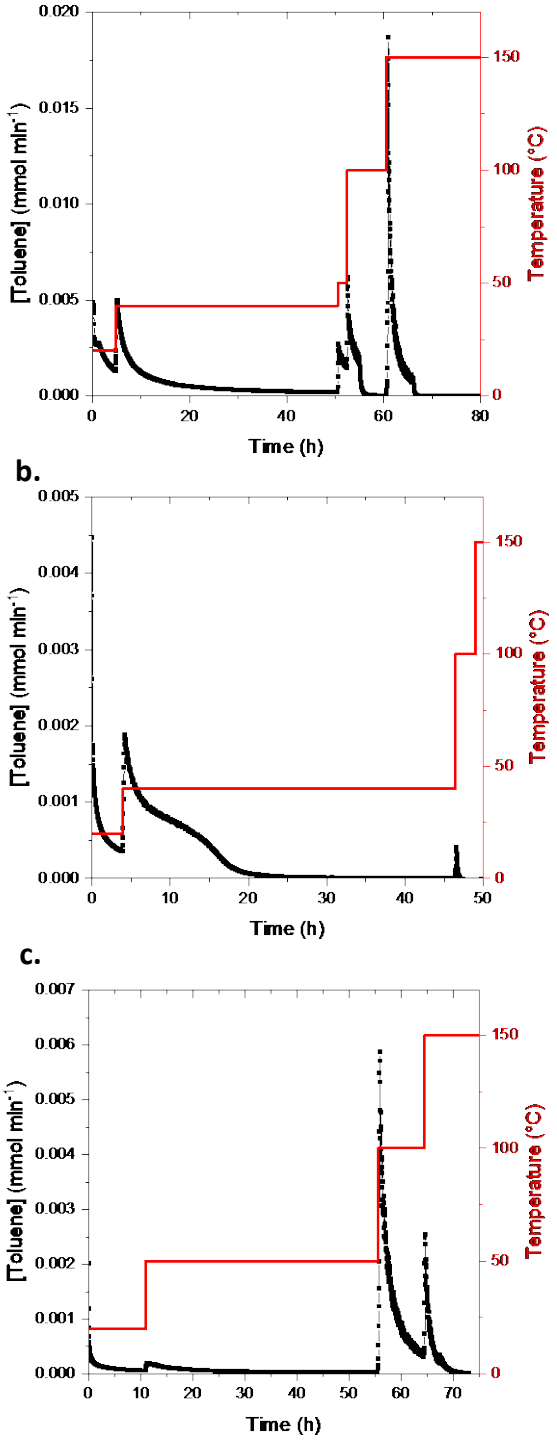

Figure 4. Desorption profiles at different temperatures of toluene previously adsorbed on AC (a), ZIF-7 (b) and ZIF-8 (c) using a dry flow (no toluene and no RH) of 200 mL min^{-1}. Bed of the adsorbent = 8 cm height. *Time is reported for 1 gram of adsorbent.

IV. DISCUSSION

The desorption profiles reveal distinct interactions between toluene and the three studied adsorbents (ZIF-7, ZIF-8 and AC). The adsorption and desorption of VOCs on AC have been extensively documented in the literature, with two primary parameters governing the sorption process: *i*) surface chemical functionalization and *ii*) pore size distribution.[26,43,44] Additional factors such as bulk density also influence sorption properties. Regarding surface functionalization, the presence of O- and N-functional groups (e.g., carboxyl, hydroxyl, amide, amine) may facilitate adsorption. O-functionalized groups are particularly crucial for the adsorption of hydrophilic adsorbates. Conversely, these groups can inhibit interactions between hydrophobic adsorbates and π-electron regions of the AC.[45] The influence of pore size is predominantly characterized by the presence of narrow micropores (< 7 Å), which dominate VOC adsorption and serve as a more reliable indicator of adsorption capacity. While mesopores facilitate faster adsorbate diffusion within the porous system, optimal adsorption occurs when the pore size closely matches the adsorbate size. The AC used as a reference in this study lacks N-functional groups but contains 2% oxygen, resulting in hydrophilic groups that enable water adsorption in the form of isolated water clusters. The primary pore size distribution, modeled using the Grand Canonical Monte Carlo (GCMC) technique for CO_2 adsorption at 298 K, is centered around 6 Å, with AC also exhibiting larger micropores (Figure S8). This broad pore size distribution explains the wide range of temperatures required for complete toluene desorption.

For ZIF-7, weak interactions between the adsorbate and adsorbent are evidenced, as a significant quantity of molecules desorb at low temperatures. At low concentrations, typically 1000 ppm ($P/P_0 = 0.037$), toluene adsorption occurs in the six-membered ring cavities of ZIF-7 in the phase II (narrow pore, np) configuration. Isotherm data at this concentration indicate

the adsorption of only two molecules per SOD cage, thus suggesting that the phase transition to phase I (large pore, lp) has not yet occurred. The adsorption process is reversible for low concentrations, as shown by the desorption branch almost superposing the adsorption branch. With only two out of a possible 15 molecules adsorbed per cage, confinement effects are minimal, facilitating easy desorption of the molecules. A temperature of 50°C is sufficient to initiate significant desorption, while heating to 100°C results in the complete desorption of all adsorbed toluene molecules.

Conversely, when adsorbing toluene in ZIF-8, minimal desorption occurs at temperatures up to 50°C in the column flushed by N_2, indicating strong interactions between the MOF and the aromatic adsorbate. This result is consistent with the flat desorption branch observed in the isotherm measurements. To complete the adsorption mechanism picture, experiments were conducted using cyclohexane, a non-aromatic molecule with a similar kinetic diameter of 6 Å, with static experiments revealing no adsorption of cyclohexane (Figure S9a). While this lack of adsorption could be attributed to an unreached thermodynamic equilibrium, dynamic experiments using a column confirmed that cyclohexane is not adsorbed on ZIF-8, resulting in an instantaneous breakthrough (Figure S9b). These findings are consistent with those of Jansen *et al.*, who observed cyclohexane adsorption only at high relative pressures, likely due to interparticle adsorption in nanocrystals.[46] Furthermore, bulky molecules such as *o*-xylene and mesitylene (kinetic diameters of 6.8 and 7.6 Å, respectively) can also be adsorbed on ZIF-8, albeit with extremely long equilibration times due to diffusional constraints.[47] These diffusional constraints are confirmed by modeling the adsorption of various adsorbates with molecular diameters up to 7 Å.[48,49] Consequently, the mechanism governing toluene adsorption on ZIF-8 is not related to molecular sieving, suggesting that an alternative adsorption mechanism governs the adsorption phenomena.

Concurrently, π-π stacking interactions between aromatic adsorbates and adsorbents during the adsorption process have been widely demonstrated in various systems, including benzene on the family of MOF-5[50] and IRMOFs,[51] and *p*-arsanilic acid on MIL-68 and UiO-66.[52,53]

As already mentioned, ZIF-8 is renowned for its gate-opening mechanism involving the rotation of the imidazolate linkers.[32,54] Kolokolov *et al.* proposed that this rotational motion can be induced by the presence of guest molecules near the six-membered ring windows, facilitating the diffusion of molecules with kinetic diameters larger than 5 Å,[55] such as toluene. Further investigations by Ueda *et al.* revealed that a flip angle of 17.6° results in the maximum opening diameter of the six-membered ring windows.[56]

Regarding toluene adsorption on ZIF-8, we propose that π-π stacking interactions, primarily governed by van der Waals forces,[57] play a crucial role. These interactions between the guest molecule and the framework facilitate the rotation of the 2-methylimidazole linker, enabling the entry of the adsorbate molecule into the sodalite cages of ZIF-8 and its subsequent diffusion within the MOF. The equilibrium times are expected to be relatively long, as only specific rotational angles of the linkers allow the diffusion of bulky molecules into the SOD cages.[58] Furthermore, increasing the BTX loading of the SOD cages may slow down diffusion as a result of beneficial guest-guest interactions in the cages, as recently proposed by Schmidt *et al.* for ethane in ZIF-8.[59] Consequently, the diffusion of aromatic molecules in ZIF-8 can be described by a local dynamic motion mechanism characterized by two aspects: *i*) a diffusion-controlled mechanism, requiring the overcoming of the high energy barrier to cross the narrow six-membered ring, and *ii*) a thermodynamically-driven mechanism, in which the host-guest interactions limit the rotation of the linker and hence increase the energy barrier. Conversely, the desorption of aromatic molecules is energy demanding due to the narrow apertures of the

six-membered ring windows and the guest-host interaction induced by π-π stacking interactions between aromatic compounds and the MOF.

V. CONCLUSION

Adsorption and desorption of BTX compounds over different ZIFs were investigated using the static method, and breakthrough experiments were performed using toluene as the adsorbate. The results have been compared to those obtained for commercial AC. To mimic relevant adsorption conditions, dynamic experiments were also conducted under humid conditions (70% RH). ZIF-7 demonstrated a remarkable ability to desorb over 90% of toluene at temperatures as low as 40°C. From an industrial perspective, this low desorption temperature poses a risk, as high concentrations of CMR (carcinogenic, mutagenic and reprotoxic) compounds would be released upon exposure to a moderate heat source such as solar radiation. In contrast, while commercial AC can adsorb higher concentrations of pollutants, its adsorption capacity is negatively affected by an amount of water vapor corresponding to a typical indoor relative humidity level. Additionally, AC desorbs a significant amount of BTX at ambient temperatures (approximately 50%), corresponding to several millimoles per gram. ZIF-8 presents an attractive alternative to AC because its adsorption of BTX is not influenced by moisture. Importantly, no significant desorption of BTX occurs at temperatures below 50°C, which is a crucial criterion for indoor air-treatment applications. When exposed to higher temperatures, ZIF-8 exhibits excellent regeneration characteristics, with only 11% of the adsorbed molecules remaining after a desorption carried out at 100°C. We propose here that the local mobility of the linker triggered (off) by guest-host interactions is responsible for the difficult desorption of toluene from ZIF-8. The publication of recent articles addressing the scalable and greener synthesis of ZIF-8 suggests that the use of ZIF-8 as an adsorbent for BTX pollutants will be highly feasible in the coming years. Due to its high retention capacity for aromatic molecules at moderate temperatures, it is even possible to envision ZIF-8 replacing activated carbon for this application.

VI. AUTHOR CONTRIBUTIONS

Thibaud Aumond: Data curation; Formal analysis; Investigation; Methodology; Resources; Software; Validation; Supervision; Visualization; Writing - original draft; Writing - review & editing. **Cécile Daniel:** Investigation; Methodology; Resources; Supervision; Validation. **Corentin Collomb:** Formal analysis; Investigation; Methodology. **Kevin Dedecker:** Investigation; Methodology; Resources. **Martin Drobek:** Investigation; Methodology; Resources. **Anne Julbe:** Investigation; Methodology; Resources. **David Farrusseng:** Methodology; Resources; Validation; Funding acquisition; Project administration; Supervision; Writing - review & editing.

VII. CONFLICTS OF INTEREST

The authors declare that they have no known competing financial interests or personal relationships that could have appeared to influence the work reported in this paper.

VIII. ACKNOWLEDGEMENTS

This research was funded by Agence Nationale de la Recherche, grant number ANR-20-CE04-0012.

IX. SUPPLEMENTARY INFORMATION

Supplementary information is available from the website about the characterization of the materials, the calibration curve used for breakthrough experiments, static adsorption

experiments of water and toluene, breakthrough experiments of toluene on activated carbon (AC) in the absence of humidity, the pore size distribution of AC, and cyclohexane adsorption on ZIF-8. The authors have cited additional references within the Supporting Information.[60, 61, 62, 63]

X. REFERENCES

[1] M. Woellner, S. Hausdorf, N. Klein, P. Mueller, M. W. Smith, S. Kaskel, Adsorption and Detection of Hazardous Trace Gases by Metal–Organic Frameworks, *Adv. Mater.*, **2018**, 30, 37, 1704679. DOI: 10.1002/adma.201704679

[2] K. Isinkaralar, G. Gullu, A. Turkyilmaz, Experimental study of formaldehyde and BTEX adsorption onto activated carbon from lignocellulosic biomass. *Biomass Conv. Bioref.* **2023**, 13, 4279–4289. DOI: 10.1007/s13399-021-02287-y

[3] H. Lahlou, X. Vilanova, X. Correig, Gas phase micro-preconcentrators for benzene monitoring: A review, *Sensors and Actuators B: Chemical*, **2013**, 176, 198-210. DOI: 10.1016/j.snb.2012.10.004

[4] M. Ali Zahed, S. Salehi, M. A. Khoei, P. Esmaeili, L. Mohajeri, Risk assessment of Benzene, Toluene, Ethylbenzene, and Xylene (BTEX) in the atmospheric air around the world: A review, *Toxicology in Vitro*, **2024**, 98, 105825. DOI: 10.1016/j.tiv.2024.105825

[5] T. He, X.-J. Kong, Z.-X. Bian, Y.-Z. Zhang, G.-R. Si, L.-H. Xie, X.-Q. Wu, H. Huang, Z. Chang, X.-H. Bu, M. J. Zawarotko, Z.-R. Nie, J.-R. Li, Trace removal of benzene vapour using double-walled metal–dipyrazolate frameworks, *Nature Materials*, **2022**, 21, 689-695. DOI: 10.1038/s41563-022-01237-x

[6] R. R. Buchholz, M. Park, H. M. Worden, W. Tang, D. P. Edwards, B. Gaubert, M. N. Deeter, T. Sullivan, M. Ru, M. Chin, R. C. Levy, B. Zheng, S. Magzamen, New seasonal pattern of pollution emerges from changing North American wildfires, *Nat. Commun.*, **2022**, 13, 2043. DOI: 10.1038/s41467-022-29623-8

[7] A. C. Lewis, D. Jenkins, C. J. M. Whitty, Hidden harms of indoor air pollution — five steps to expose them, *Nature*, **2023**, 614, 220-223. DOI: 10.1038/d41586-023-00287-8

[8] G. Lee, S. No, K. Kim, C. Jo, Post-treatment of carbon by interparticle spillover hydrogen for sustainable adsorption of volatile organic compounds under humid conditions, *Chemical Engineering Journal*, **2023**, 477, 147028. DOI: 10.1016/j.cej.2023.147028

[9] Y. Yang, C. Sun, B. Lin, Q. Huang, Surface modified and activated waste bone char for rapid and efficient VOCs adsorption, *Chemosphere*, **2020**, 256, 127054. DOI: 10.1016/j.chemosphere.2020.127054

[10] H. Zhang, L. Zhu, Z. Pan, J. Cui, B. Wang, D. Zhang, Y. Guo, F. Cheng, Exploring the mechanisms of enhanced activated carbon's toluene adsorption and regeneration by utilizing inherent pyrite in coal, *Fuel*, **2025**, 386, 134224. DOI: 10.1016/j.fuel.2024.134224

[11] B. S. Bal'zhinimaev, E. A. Paukshtis, A. V. Toktarev, E. V. Kovalyov, M. A. Yaranova, A. E. Smirnov, S. Stompel, Effect of water on toluene adsorption over high silica zeolites, 2019, *Microporous and Mesoporous Materials*., **2019**, 277, 70. DOI: 10.1016/j.micromeso.2018.10.023

[12] H. Deng, T. Pan, Y. Zhang, L. Wang, Q. Wu, J. Ma, W. Shan, H. He, Adsorptive removal of toluene and dichloromethane from humid exhaust on MFI, BEA and FAU zeolites: An experimental and theoretical study, *Chemical Engineering Journal*, **2020**, 394, 124986. DOI: 10.1016/j.cej.2020.124986

[13] S. Zhang, L. Yao, B. Xu, L. Yang, Z. Dai, W. Jiang, Recent advances in zeolite-based materials for volatile organic compounds adsorption, *Separation and Purification Technology*, **2024**, 350, 127742. DOI: 10.1016/j.seppur.2024.127742

[14] C.-A. Roulet, M.-C. Pibiri, R. Knutti, A. Pfeiffer, A. Weber, Effect of chemical composition on VOC transfer through rotating heat exchangers, *Energy and Buildings*, **2002**, 34, 799-807. DOI: 10.1016/S0378-7788(02)00098-1

[15] J. E. Szulejko, K.-H. Kim, J. Parise, Seeking the most powerful and practical real-world sorbents for gaseous benzene as a representative volatile organic compound based on performance metrics, *Separation and Purification Technology*, **2019**, 212, 980-985. DOI: 10.1016/j.seppur.2018.11.001

[16] Z. X. Zhao, X. M. Li, Z. Li, Chemical Engineering Journal, Adsorption equilibrium and kinetics of p-xylene on chromium-based metal-organic framework MIL-1012011, 173, 150. DOI: 10.1016/j.cej.2011.07.051

[17] X. Zhang, Y. Yang, X. Lv, Y. Wang, N. Liu, D. Chen, L. Cui, Adsorption/desorption kinetics and breakthrough of gaseous toluene for modified microporous-mesoporous UiO-66 metal organic framework, *Journal of Hazardous Materials*, **2019**, 366, 140. DOI: 10.1016/j.jhazmat.2018.11.099

[18] K. Vellingiri, P. Kumar, A. Deep, K.-H. Kim, Metal-organic frameworks for the adsorption of gaseous toluene under ambient temperature and pressure, *Chemical Engineering Journal*, **2017**, 307, 1116. DOI: 10.1016/j.cej.2016.09.012

[19] B. Siu, A. R. Chowdhury, Z. Yan, S. M. Humphrey, T. Hutter, Selective adsorption of volatile organic compounds in metal-organic frameworks (MOFs), *Coordination Chemistry Reviews*, **2023**, 485, 215119. DOI: 10.1016/j.ccr.2023.215119

[20] L. Zhu, D. Shen, K. H. Luo, A critical review on VOCs adsorption by different porous materials: Species, mechanisms and modification methods, *Journal of Hazardous Materials*, **2020**, 389, 122102. DOI: 10.1016/j.jhazmat.2020.122102

[21] J. Canivet, A. Fateeva, Y. Guo, B. Coasne, D. Farrusseng, Water adsorption in MOFs: fundamentals and Applications, *Chem. Soc. Rev.*, **2014**, 43, 5594. DOI: 10.1039/C4CS00078A

[22] N. C. Burtch, H. Jasuja, K. S. Walton, Water Stability and Adsorption in Metal−Organic Frameworks, *Chem. Rev.*, **2014**, 114, 10575. DOI: 10.1021/cr5002589

[23] L.-H. Xie, M.-M. Xu, X.-M. Liu, M.-J. Zhao, J.-R. Li, Hydrophobic Metal–Organic Frameworks: Assessment, Construction, and Diverse Applications, *Adv. Sci.*, **2020**, 7, 1901758. DOI: 10.1002/advs.201901758

[24] M. Trčka, J. L. M. Hensen, Overview of HVAC system simulation, *Automation in Construction*, **2010**, 19, 93-99. DOI: 10.1016/j.autcon.2009.11.019

[25] S. Taheri, P. Hosseini, A. Razban, Model predictive control of heating, ventilation, and air conditioning (HVAC) systems: A state-of-the-art review, *Journal of Building Engineering*, **2022**, 60, 105067. DOI: 10.1016/j.jobe.2022.105067

[26]X. Yang, H. Yi, X. Tang, S. Zhao, Z. Yang, Y. Ma, T. Feng, X. Cui, Behaviors and kinetics of toluene adsorption-desorption on activated carbons with varying pore structure, *Journal of environmental science*, **2018**, 67, 104-114. DOI: 10.1016/j.jes.2017.06.032

[27] E. Alvarez, Traitement de l'air habitacle par des matériaux hybrides de type Metal-Organic Frameworks. Ph.D. Dissertation, Paris-Saclay University, Institut Lavoisier de Versailles, 2016. https://theses.fr/2016SACLV006 (accessed 2024-11-27).

[28] R. A. Klein, S. Shulda, P. A. Parilla, P. Le Magueres, R. K. Richardson, W. Morris, C. M. Brown, C. M. McGuirk, Structural resolution and mechanistic insight into hydrogen adsorption in flexible ZIF-7, *Chem. Sci.*, **2021**, 12, 15620-15631. DOI: 10.1039/D1SC04618G

[29] P. Iacomi, G. Maurin, ResponZIF Structures: Zeolitic Imidazolate Frameworks as Stimuli-Responsive Materials, *ACS Appl. Mater. Interfaces*, **2021**, 13, 43, 50602–50642. DOI: 10.1021/acsami.1c12403

[30] A. U. Ortiz, A. P. Freitas, A. Boutin, A. H. Fuchs, F.-X. Coudert, What Makes Zeolitic Imidazolate Frameworks Hydrophobic or Hydrophilic? Impact of Geometry and Functionalization on Water Adsorption, *Phys. Chem. Chem. Phys.*, **2014**, 16, 9940. DOI: 10.1039/C3CP54292K

[31] C. Cuadrado-Collados, J. Fernández-Català, F. Fauth, Y. Q. Cheng, L. L. Daemen, A. J. Ramirez-Cuesta, J. Silvestre-Albero, Understanding the breathing phenomena in nano-ZIF-7 upon gas adsorption, *J. Mater. Chem. A.*, **2017**, 5, 20938. DOI: 10.1039/c7ta05922a

[32] D. Fairen-Jimenez, S. A. Moggach, M. T. Wharmby, P. A. Wright, S. Parsons, T. Düren, Opening the Gate: Framework Flexibility in ZIF-8 Explored by Experiments and Simulations. *J. Am. Chem. Soc.*, **2011**, 113, 8900-8902. DOI: 10.1021/ja202154j

[33] R. Boada, J. Chaboy, S. Hayama, L.L Keenan, A.A. Freeman, M. Amboage, S. Díaz-Moreno, Unraveling the Molecular Details of the "Gate Opening" Phenomenon in ZIF-8 with X-ray Absorption Spectroscopy. *J. Phys. Chem. C*, **2022**, 126, 5935-5943. DOI: 10.1021/acs.jpcc.2c00373

[34] P. Zhao, H. Fang, S. Mukhopadhyay, A. Li, S. Rudic, I. J. McPherson, C. C. Tang, D. Fairen-Jimenez, S. C. E. Tsang, S. A. T. Redfern, Structural dynamics of a metal–organic framework induced by CO2 migration in its non-uniform porous structure, *Nat. Commun.*, **2019**, 10, 999. DOI: 10.1038/s41467-019-08939-y

[35] Y. Du, B. Wooler, M. Nines, P. Kortunov, C. S. Paur, J. Zengel, S. C. Weston, P. I. Ravikovitch, New High- and Low-Temperature Phase Changes of ZIF-7: Elucidation and

Prediction of the Thermodynamics of Transitions, *J. Am. Chem. Soc.*, **2015**, 137, 42, 13603-13611. DOI: 10.1021/jacs.5b08362

[36] S. Aguado, G. Bergeret, M. P. Titus, V. Moizan, C. Nieto-Draghi, N. Bats, D. Farrusseng, Guest-induced gate-opening of a zeolite imidazolate framework, *New J. Chem.*, **2011**, 35, 546-550. DOI: 10.1039/C0NJ00836B

[37] D.-L. Chen, N. Wang, F.-F. Wang, J. Xie, Y. Zhong, W. Zhu, J. K. Johnson, R. Krishna, Utilizing the Gate-Opening Mechanism in ZIF-7 for Adsorption Discrimination between N_2O and CO_2, *J. Phys. Chem. C*, **2014**, 118, 31, 17831-17837. DOI: 10.1021/jp5056733

[38] Y.-T. Zhao, L.-Q. Yu, X. Xia, X.-Y. Yang, W. Hu, Y.-K. Lv, Evaluation of the adsorption and desorption properties of zeolitic imidazolate framework-7 for volatile organic compounds through thermal desorption-gas chromatography, *Anal. Methods*, **2018**, 10, 4894-4901. DOI: 10.1039/C8AY01856A

[39] T. Aumond, R. Manokaran, J. Eck, O. Ergincan, C. Daniel, D. Farrusseng, B. Coasne, A Review on Adsorption in Nanoporous Adsorbents for Gas Decontamination: Space Applications and Beyond, *Ind. Eng. Chem. Res.* **2024**, 63, 45, 19375–19397. DOI: 10.1021/acs.iecr.4c02052

[40] D. Ursueguía, C. Daniel, C. Collomb, C. Cardenas, D. Farrusseng, E. Díaz, S. Ordóñez, Evaluation of HKUST-1 as Volatile Organic Compound Adsorbents for Respiratory Filters, *Langmuir*, **2022**, 38, 47, 14465–14474. DOI: 10.1021/acs.langmuir.2c02332

[41] O. C. Gobin, S. J. Reitmeier, A. Jentys, J. A. Lercher, Diffusion pathways of benzene, toluene and p-xylene in MFI, *Microporous and Mesoporous Materials*, **2009**, 125, 3. DOI: 10.1016/j.micromeso.2009.01.025

[42] L. Liu, S. J. Tan, T. Horikawa, D. D. Do, D. Nicholson, J. Liu, Water adsorption on carbon – A review, *Adv. Colloid and surf. Sci.*, **2017**, 250, 64. DOI: 10.1016/j.cis.2017.10.002

[43] X. Zhang, B. Gao, A. E. Creamer, C. Cao, Y. Li, Adsorption of VOCs onto engineered carbon materials: A review, *Journal of Hazardous Materials*, **2017**, 338, 102-123. DOI: 10.1016/j.jhazmat.2017.05.013

[44] M. A. Lillo-Ródenas, D. Cazorla-Amorós & A. Linares-Solano, Benzene and toluene adsorption at low concentration on activated carbon fibres, *Adsorption*, **2011**, 17, 473–481. DOI: 10.1007/s10450-010-9301-7

[45] M.A. Lillo-Ródenas, D. Cazorla-Amorós, A. Linares-Solano, Behaviour of activated carbons with different pore size distributions and surface oxygen groups for benzene and toluene adsorption at low concentrations, *Carbon* **2005**, 43, 1758–1767. DOI: 10.1016/j.carbon.2005.02.023

[46] C. Jansen, N. Assahub, A. Spieß, J. Liang, A. Schmitz, S. Xing, S. Gökpinar, C. Janiak, The Complexity of Comparative Adsorption of C6 Hydrocarbons (Benzene, Cyclohexane, n-Hexane) at Metal–Organic Frameworks. *Nanomaterials* **2022**, 12, 3614. DOI: 10.3390/nano12203614

[47] K. Zhang, R. P. Lively, C. Zhang, R. R. Chance, W. J. Koros, D. S. Sholl, S. Nair, Exploring the Framework Hydrophobicity and Flexibility of ZIF-8: From Biofuel Recovery to Hydrocarbon Separations. *J. Phys. Chem. Lett.* **2013**, 4, 21, 3618–3622. DOI: 10.1021/jz402019d

[48] R. J. Verploegh, S. Nair, D. S. Sholl, Temperature and Loading-Dependent Diffusion of Light Hydrocarbons in ZIF-8 as Predicted Through Fully Flexible Molecular Simulations, *J. Am. Chem. Soc.*, **2015**, 137, 15760−15771. DOI: 10.1021/jacs.5b08746

[49] R. J. Verploegh, A. Kulkarni, S. E. Boulfelfel, J. C. Haydak, D. Tang, D. S. Sholl, Screening Diffusion of Small Molecules in Flexible Zeolitic Imidazolate Frameworks Using a DFT-Parameterized Force Field, *J. Phys. Chem. C*, **2019**, 123, 9153-9167. DOI: 10.1021/acs.jpcc.9b00733

[50] S. Amirjalayer, R. Schmid, Mechanism of benzene diffusion in MOF-5: A molecular dynamics investigation. *Microporous Mesoporous Mater.*, **2009**, 125, 90-96. DOI: 10.1016/j.micromeso.2009.02.006

[51] K. Dedecker, M. Drobek, A. Julbe, Effect of Ligand Aromaticity on Cyclohexane and Benzene Sorption in IRMOFs: A Computational Study. *J. Phys. Chem. B*, **2023**, 127, 51, 11091-11099. DOI: 0.1021/acs.jpcb.3c06886

[52] Y. Lv, R. Zhang, S. Zeng, K. Liu, S. Huang, Y. Liu, P. Xu, C. Lin, Y. Cheng, M. Liu, Removal of p-arsanilic acid by an amino-functionalized indium-based metal–organic framework: Adsorption behavior and synergetic mechanism. *Chemical Engineering Journal*, **2018**, 339, 359-368. DOI: 10.1016/j.cej.2018.01.139

[53] C. Tian, J. Zhao, X. Ou, J. Wan, Y. Cai, Z. Lin, Z. Dang, B. Xing, Enhanced Adsorption of p-Arsanilic Acid from Water by Amine-Modified UiO-67 as Examined Using Extended X-ray Absorption Fine Structure, X-ray Photoelectron Spectroscopy, and Density Functional Theory Calculations. *Environ. Sci. Technol.* **2018**, 52, 3466−3475. DOI: 10.1021/acs.est.7b05761

[54] S. Tanaka, K. Fujita, Y. Miyake, M. Miyamoto, Y. Hasegawa, T. Makino, S. van der Perre, J. Cousin Saint-Remi, T. van Assche, G. V. Baron, J. F. M. Denayer, Adsorption and Diffusion Phenomena in Crystal Size Engineered ZIF-8 MOF, *J. Phys. Chem. C,* **2015**, 119, 51, 28430–28439. DOI: 10.1021/acs.jpcc.5b09520

[55] D. I. Kolokolov, A. G. Stepanov, H. Jobic, Mobility of the 2-Methylimidazolate Linkers in ZIF-8 Probed by ^{2}H NMR: Saloon Doors for the Guests. *J. Phys. Chem. C* **2015**, 119, 27512−27520. DOI: 10.1021/acs.jpcc.5b09312

[56] T. Ueda, T. Yamatani, M. Okumura, Dynamic Gate Opening of ZIF-8 for Bulky Molecule Adsorption as Studied by Vapor Adsorption Measurements and Computational Approach. *J. Phys. Chem. C*, **2019**, 123, 27542-27553.

[57] C.A. Hunter, J.K.M. Sanders, The Nature of π-π Interactions. *J. Am. Chem. Soc.*, **1990**, 112, 5525-5534. DOI: 10.1021/ja00170a016

[58] A. E. Khudozhitkov, H. Zhao, A. Ghoufi, S. S. Arzumanov, D. I. Kolokolov, G. Maurin, A. G. Stepanov, Molecular Insight into the Slow Dynamics of C4 Hydrocarbons in the Zeolitic−Imidazole Framework (ZIF-8), *ACS Appl. Mater. Interfaces* **2021**, 13, 33685−33692. DOI: 10.1021/acsami.1c08529

[59] B. E. Schmidt, P. Cnudde, V. Van Speybroeck, L. Vanduyfhuys, In-Depth Thermodynamic and Kinetic Analysis of Ethane Diffusion in ZIF-8, *J. Phys. Chem. C*, **2024**, 128, 18509-18523. DOI: 10.1021/acs.jpcc.4c04790

[60] W. Cai, T. Lee, W. Cho, D. Y. Han, N. Choi, A. C. K. Yip, J. Choi, Thermal Structural Transitions and Carbon Dioxide Adsorption Properties of Zeolitic Imidazolate Framework-7 (ZIF-7), *J. Am. Chem. Soc.* **2014**, 136, 22, 7961–7971. DOI: 10.1021/ja5016298

[61] K. Kida, M. Okita, K. Fujita, S. Tanaka, Y. Miyake, Formation of high crystalline ZIF-8 in an aqueous Solution, *Cryst. Eng. Comm.* **2013**, 15, 1794. DOI: 10.1039/C2CE26847G

[62] M. He, J. Yao, L. Li, K. Wang, F. Chen, H. Wang, Synthesis of Zeolitic Imidazolate Framework-7 in a Water/Ethanol Mixture and Its Ethanol-Induced Reversible Phase Transition. *ChemPlusChem* **2013**, 78, 1222-1225. DOI: 10.1002/cplu.201300193

[63] W. Morris, N. He, K. G. Ray, P. Klonowski, H. Furukawa, I. N. Daniels, Y. A. Houndonougbo, M. Asta, O. M. Yaghi, B. B. Laird, A Combined Experimental-Computational Study on the Effect of Topology on Carbon Dioxide Adsorption in Zeolitic Imidazolate Frameworks. *J. Phys. Chem. C* **2012**, 116, 45, 24084–24090. DOI: 10.1021/jp307170a